Rev. Roum. Sci. Techn.– Électrotechn. et Énerg.
Vol. **61**, *3*, pp. 263–268, Bucarest, 2016

A NOVEL DIRECT POWER CONTROL FOR GRID-CONNECTED DOUBLY FED INDUCTION GENERATOR BASED ON HYBRID ARTIFICIAL INTELLIGENT CONTROL WITH SPACE VECTOR MODULATION

FAYSSAL AMRANE[1,*], AZEDDINE CHAIBA[1]

Key words: Direct power control (DPC), Doubly fed induction generator (DFIG), Space vector modulation (SVM), Model reference adaptive control (MRAC), Type2 fuzzy logic control (T2FLC), Neuro fuzzy control (NFC), Maximum power point tracking (MPPT).

This paper presents a novel direct power control (DPC) for doubly fed induction generator (DFIG), based on hybrid artificial intelligent with a fixed switching frequency for wind generation application via maximum power point tracking (MPPT) strategy. First, a mathematical model of the DFIG written in an appropriate d-q reference frame is established to investigate simulations. A control law based on direct power control is synthesized using only PID controllers. To improve the performance of our system, we propose model reference adaptive control (MRAC), type2 fuzzy logic control (T2FLC) and neuro-fuzzy control (NFC), to control rotor current. Results obtained using MATLAB/Simulink environment with/without MPPT strategy, are discussed in details; have shown high efficiency and high dynamics.

1. **INTRODUCTION**

Wind energy conversion system (WECSs) based on the doubly-fed induction generator (DFIG) dominated the wind power generations due to the outstanding advantages, including small converters rating around 30% of the generator rating, lower converter cost. Several novel control strategies have been investigated in order to improve the DFIG operation performance [1-2]. Nowadays, since DFIG-based WECSs are mainly installed in remote and rural areas [2]. In literature [3] vector control is the most popular method used in the DFIG-based WTs.

The DPC is simple and alternative approach control formulation that does not require decomposition into symmetrical components; the DPC schemes have been proved to be preponderant for DFIGs due to the simple implementation [4]. A schematic diagram of wind turbine system with a DFIG is shown in fig.1.

In [5], the author has proposed a new modeling approach for DFIG, for develop the state vector including directly as states the stator circuit and grid side converter. In [6] a direct power control (DPC) of a single voltage source converter based on doubly fed induction generator (DFIG) without using a rotor position sensor. Simulation and experimental results of a 3.7 kW DFIG system are presented to demonstrate the performance of the proposed WECS under steady state. In [7], the authors have presented a model reference adaptive control (MRAC) speed estimator for speed sensorless direct torque and flux control of an induction motor, propose tow topologies based in Type-1fuzzy logic controller (T1FLC) and Type-2 fuzzy logic controller (T2FLC) to achieve high performance sensorless drive. In [8], a statistic study has proposed, which based on applications of fuzzy logic in renewable energy systems between 1994 until 2014. We remark that the wind energy had the big importance in these researches using neuro fuzzy, fuzzy particle swarm optimization, fuzzy genetic algorithms in simulation and experimental. In [9], the authors have devoted their studies in the application of sliding mode of DFIG, for wind power generation, using the robustness tests to improve the system performances. Other advantages of MRAC are it has the ability to control the system that undergoes parameter and/or environmental variations. Fuzzy-neural techniques are proposed for electrical drives in details in [10].

This paper is organized as follows; firstly the modeling of the turbine is presented in section 2. In section 3, the mathematical model of DFIG is given. Section 4 presents direct power control of DFIG which is based on the orientation of the stator flux vector along the axis ‘d’. The model reference adaptive control, type 2 fuzzy logic control and neuro-fuzzy control are established to control the rotor currents after being compared by conventional regulators PID in Section 5, 6 and 7 respectively. In section 8, computer simulation results are shown and discussed. Finally, the reported work is concluded.

2. **MODEL OF TURBINE**

The wind turbine input power usually is:

$$Pv = \frac{1}{2}.\sigma.S_w.V^3, \tag{1}$$

Where σ is air density; S_w is wind turbine blades swept area and V is wind speed.

The output mechanical power of wind turbine is:

$$Pm = Cp.Pv = \frac{1}{2}.Cp.\rho.S_w.V^3, \tag{2}$$

Where Cp represents power coefficient, λ is tip speed ratio and β the blade pitch angle, λ is given by:

$$\lambda = \frac{R.\Omega t}{v}, \tag{3}$$

[1,*] University of Setif 1, Department of Electrical Engineering, LAS Research Laboratory19000 Setif, Algeria. E-mail: amrane_fayssal@live.fr; chaiba_azeddine@yahoo.fr

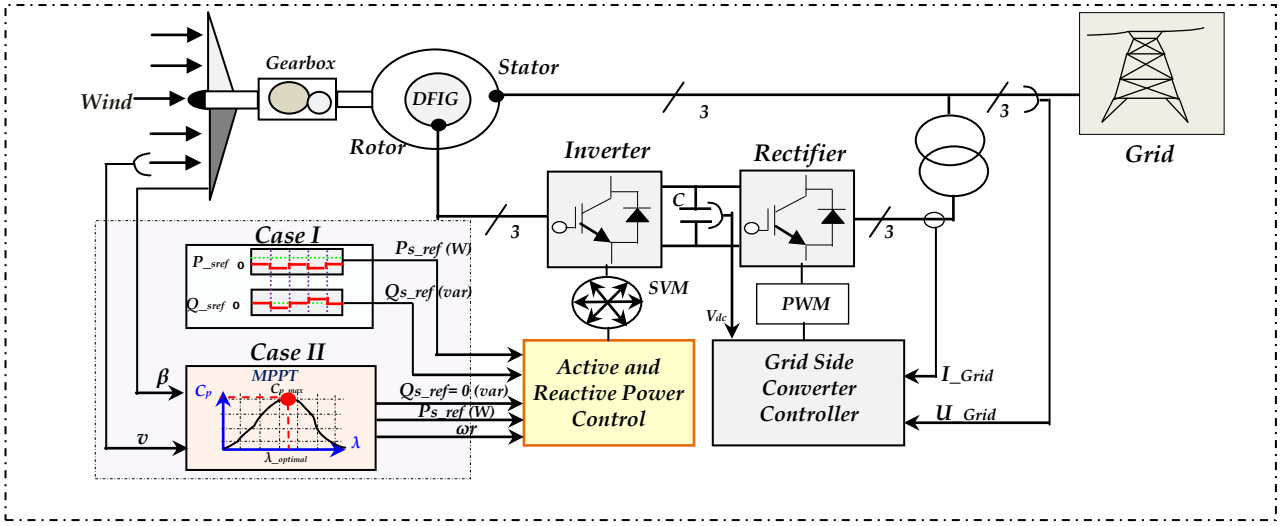

Fig. 1 –Schematic diagram of wind turbine system with DFIG.

Where R is blade radius, Ωt is angular speed of the turbine. Cp can be described as:

$$Cp = (0.5 - 0.0167.(\beta - 2)).\sin\left[\frac{\pi.(\lambda + 0.1)}{18.5 - 0.3.(\beta - 2)}\right] - (4)$$
$$0.00184.(\lambda - 3).(\beta - 2)$$

In our work, we use the wind profile, as shown in fig.3:

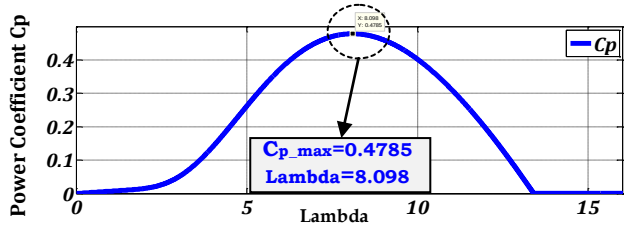

Fig. 2 – Power coefficient variation Cp against tip speed ratio λ.

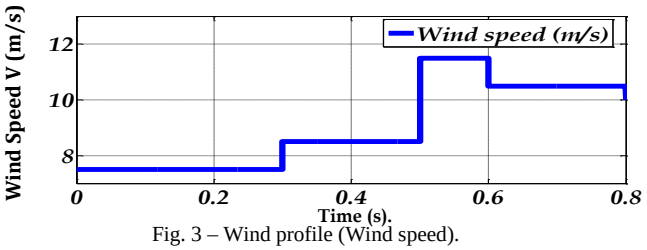

Fig. 3 – Wind profile (Wind speed).

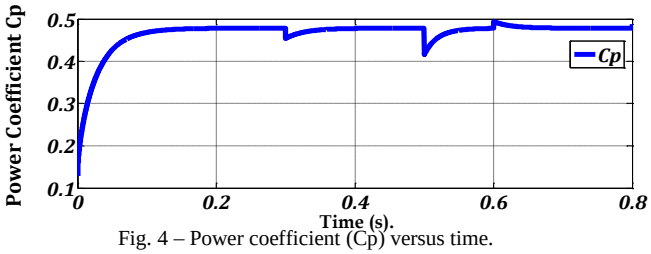

Fig. 4 – Power coefficient (Cp) versus time.

The maximum value of Cp $(Cp\_\max = 0.4785)$ is achieved for $\beta = 1.8°$ and for $\lambda_{opt} = 8.098$. This point corresponds at the maximum power point tracking (MPPT) [11] as shown in fig.2. After the simulation of the wind turbine using this wind profile (fig.3), we test the robustness of our MPPT algorithm, we have as results the curve of power coefficient Cp versus time (fig.4); this latter achieved the maximum value mentioned in fig.2 $(Cp\_\max = 0.4785)$ despite the variation of the wind.

3. MATHEMATICAL MODEL OF DFIG

The general electrical state model of the DFIG obtained using Park transformation is given by the following equations [12]:

Voltage and fluxes equations for stator and rotor respectively

$$\begin{cases} Vsd = Rs.Isd + \dfrac{d}{dt}\phi sd - \omega s.\phi sq \\ Vsq = Rs.Isq + \dfrac{d}{dt}\phi sq - \omega s.\phi sd \\ Vrd = Rr.Ird + \dfrac{d}{dt}\phi rd - (\omega s - \omega).\phi rq \\ Vrq = Rr.Irq + \dfrac{d}{dt}\phi rq - (\omega s - \omega).\phi rd \end{cases}, \quad (5)$$

$$\begin{cases} \phi sd = Ls.Isd + Lm.Ird \\ \phi sq = Ls.Isq + Lm.Irq \\ \phi rd = Lr.Ird + Lm.Isd \\ \phi rq = Lr.Ird + Lm.Lsq \end{cases}, \quad (6)$$

The electromagnetic torque is given by:

$$\begin{cases} Ce = P.Lm.(Ird.Isq - Irq.Isd) \\ Ce - Cr = J.\dfrac{d}{dt}\Omega + f.\Omega \end{cases}, \quad (7)$$

where: Cr is the load torque, J is total inertia and Ω is mechanical speed. The voltage vectors, produced by a three-phase PWM inverter, divide the space vector plane into six sectors (fig.6), as shown in fig.5 [11].

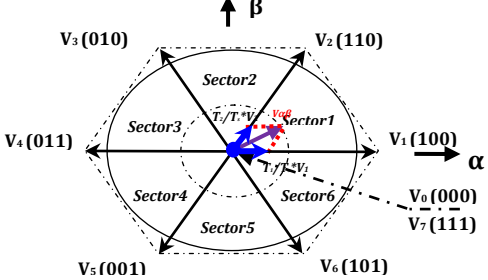

Fig. 5 – The diagram of voltage space vectors in α-β plan.

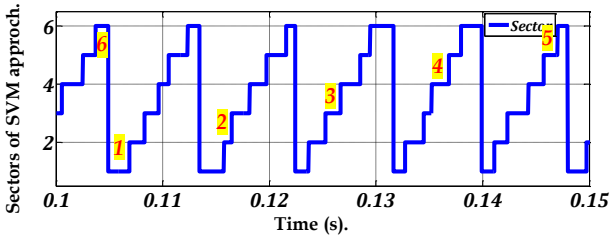

Fig. 6 – Sectors of space vector modulation (SVM) approach.

4. DIRECT POWER CONTROL OF DFIG

In this section, the DFIG model can be described by the following state equations in the synchronous reference frame whose axis d is aligned with the stator flux vector as shown in fig.7, $\phi sd = \phi s$ and $\phi sq = 0$ [13].

By neglecting resistances of the stator phases the stator voltage will be expressed by:

$$Vsd = 0 \text{ and } Vsq = Vs \cong \omega s.\phi s \tag{8}$$

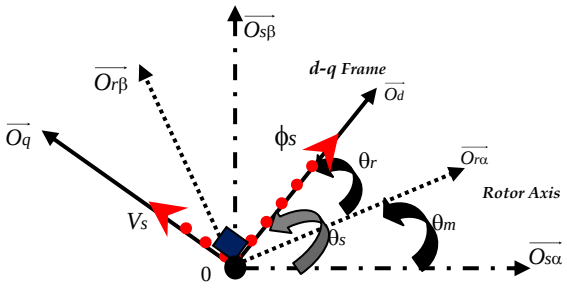

Fig. 7 – Stator and rotor flux vectors in the synchronous d-q Frame.

We lead to an uncoupled power control; where, the transversal component Irq of the rotor current controls the stator active power. The stator reactive power is imposed by the direct component Ird as in shown in fig.8 [13]:

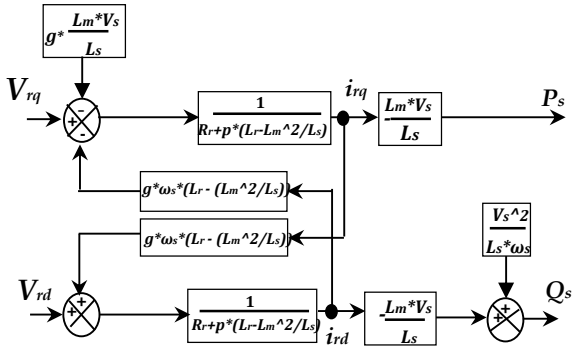

Fig. 8 – The doubly fed induction generator simplified model.

$$\begin{cases} Ps = -Vs.\dfrac{Lm}{Ls}.Irq \\ Qs = \dfrac{V_s^2}{\omega s.Ls} - Vs.\dfrac{Lm}{Ls}.Ird \end{cases}, \tag{9}$$

The arrangement of the equations gives the expressions of the voltages according to the rotor currents (fig.9):

$$\begin{cases} Vrd = Rr.Ird + (Lr - \dfrac{L_m^2}{Ls}).\dfrac{\mathrm{d}Ird}{\mathrm{d}t} \\ \quad - g.\omega s.(Lr - \dfrac{L_m^2}{Ls}).Irq \\ Vrq = Rr.Irq + (Lr - \dfrac{L_m^2}{Ls}).\dfrac{\mathrm{d}Irq}{\mathrm{d}t} \\ \quad - g.\omega s.(Lr - \dfrac{L_m^2}{Ls}).Ird + g.\dfrac{Lm.Vs}{Ls} \end{cases}, \tag{10}$$

$$\begin{cases} \dfrac{\mathrm{d}Ird}{\mathrm{d}t} = -\dfrac{1}{\sigma.Tr}.Ird + g.\omega s.Irq + \dfrac{1}{\sigma.Lr}.Vrd \\ \dfrac{\mathrm{d}Irq}{\mathrm{d}t} = -\dfrac{1}{\sigma}.(\dfrac{1}{Tr} + \dfrac{L_m^2}{Ls.Ts.Lr}).Irq - g.\omega s.Ird + \dfrac{1}{\sigma.Lr}.Vrq \end{cases} \tag{11}$$

with: $Tr = \dfrac{Lr}{Rr}; Ts = \dfrac{Ls}{Rs}; \sigma = 1 - \dfrac{L_m^2}{Ls.Lr}$

where: $\phi sd, \phi sq$ are stator flux components, $\phi rd, \phi rq$ are rotor flux components, Vsd, Vsq are stator voltage components, Vrd, Vrq are rotor voltage components. Rs, Rr are stator and rotor resistances, Ls, Lr are stator and rotor inductances, Lm is mutual inductance, σ is leakage factor, P is number of pole pairs, ωs is the stator pulsation, ω is the rotor pulsation, f is the friction coefficient, Ts and Tr are stator and rotor time-constant, and g is the slip. The conventional DPC of a DFIG based on PID is shown in fig.9.

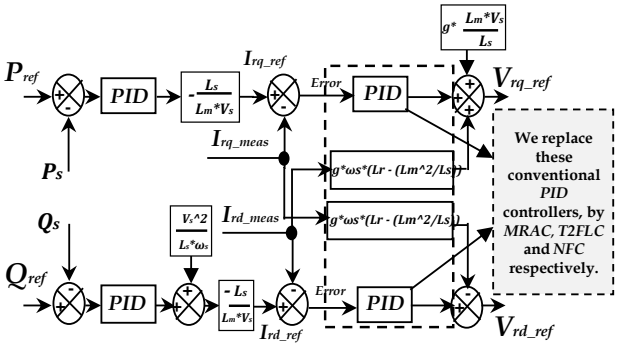

Fig. 9 – The conventional DPC of a DFIG based on PID.

5. MODEL REFERENCE ADAPTIVE CONTROL

The system studied in this paper is based on a first-order linear plant approximation given by [7-9]:

$$\dot{x}(t) = a.x(t) + b.u(t) \tag{12}$$

Where $x(t)$ is the plant state, $u(t)$ is the control signal, a and b are the plant parameters. The control signal is generated from both the state variable and the reference signal $r(t)$, multiplied by the adaptive control gains k and kr such that:

$$u(t) = k(t).x(t) + kr(t).r(t) \tag{13}$$

Where $k(t)$ is the feedback adaptive gain and $kr(t)$ the feed forward adaptive gain.

The plant is controlled to follow the output from a reference model. The equivalent scheme of MRAC for adjusting rotor currents of DPC is shown in fig.10.

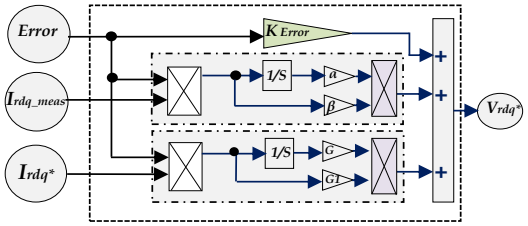

Fig. 10 – The Simulink scheme of MRAC for rotor currents.

6. DESIGN OF TYPE2 FUZZY LOGIC CONTROL

The type2 fuzzy controller utilized in this work has two inputs and one output. The membership functions are defined in fig.11 (A and B). The inferences of T2FLC can be made in a more explain as shown in table.1 [8].

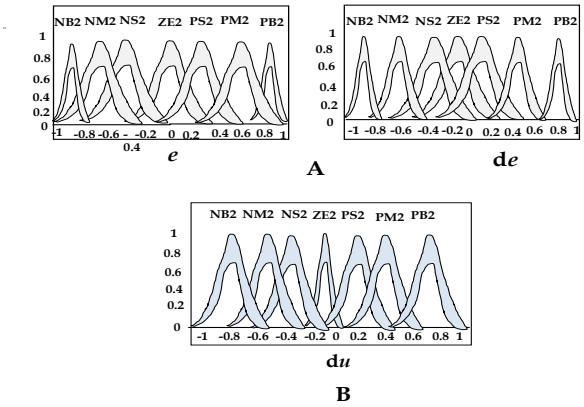

Fig. 11 – Membership functions (A: inputs and B: output).

The type2 fuzzy rule base consists of a collection of linguistic rules of the form [8]:

Rule 1: if $S_{1,2}$ is NB2, and $S_{1,2}$ is NB2 then $dU_{1,2}$ is NB2.
Rule 2: if $S_{1,2}$ is NM2, and $S_{1,2}$ is NB2 then $dU_{1,2}$ isNB2.
Rule 3: if $S_{1,2}$ is NS2, and $S_{1,2}$ is NG2 then $dU_{1,2}$ is NS2.
.
.
.
Rule 49: if $S_{1,2}$ is PB2, and $S_{1,2}$ is PB2 then $dU_{1,2}$ isPB2.

With: NB: Negative Big, NM: Negative Medium, NS: Negative Small, ZE: Zero environ, PS: Positive Small, PM: Positive Medium, PB: Positive Big and the number '2' means the type2 fuzzy logic control.

Table 1

Type2 Fuzzy logic Inferences.

dU1,2		**dS1,2**						
		NB2	**NM2**	**NS2**	**EZ2**	**PS2**	**PM2**	**PB2**
dS1, 2	**NB2**	NB2	NB2	NB2	NM2	NS2	NS2	**EZ2**
	NM2	NB2	NM2	NM2	NM2	NS2	**EZ2**	PS2
	NS2	NB2	NM2	NS2	NS2	**EZ2**	PS2	PM2
	EZ2	NB2	NM2	NS2	**EZ2**	PS2	PM2	PM2
	PS2	NM2	NS2	**EZ2**	PS2	PS2	PM2	PB2
	PM2	NS2	**EZ2**	PS2	PM2	PM2	PM2	PB2
	PB2	**EZ2**	PS2	PS2	PM2	PB2	PB2	PB2

7. DESIGN OF NEURO-FUZZY CONTROLLER

The NFC controller is composed of an on-line learning algorithm with a neuro-fuzzy network [10]. The neuro-fuzzy network is trained using an on-line learning algorithm. The NFC has two inputs, the rotor current error e_{idr} and the derivative of rotor current error $\dot{e}_{idr}$. The output is rotor voltage V_{rd}. For the NFC of rotor current I_{rq} is similar with I_{rd} controller. The neuro-fuzzy network is shown in fig.12.

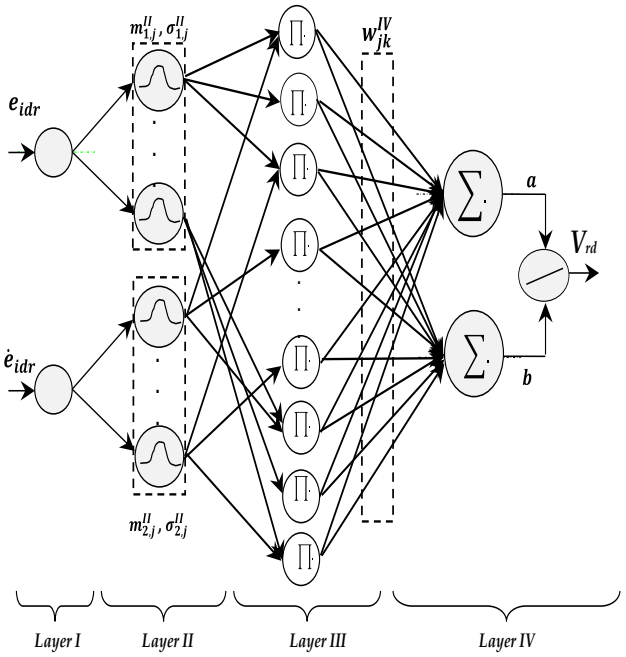

Fig. 12 – Schematic diagram of the neuro-fuzzy network.

8. SIMULATION RESULTS

The DFIG used in this work is a 4 kW whose nominal parameters are indicated in table.3. And the wind turbine used in this work is a 10 kW whose parameters are indicated in table.4.

For both cases, we use robustness test as follows:

Test 1: (Without robustness test)

Test 2: Add **100%** for Rr, and decrease **25%** for Ls, Lr, and Lm.

Test 3: Add **100 %** for Rr and J, and decrease **25%** for Ls, Lr, and Lm.

8.1 CASE I (WITHOUT MPPT STRATEGY):

Fig.13 (to the left) represents the stator active power and its reference profiles using SVM for proposed control using MRAC, T2FLC and NFC respectively; the stator active power reference is indicated in table.5. We remark that the stator active power follows exactly its reference for the three proposed controls (Test1). After a robustness test (Test 2), the stator active power follows its reference, but we note that there are a great power error and more ripples in proposed control based on MRAC, lower power error in proposed control based on T2FLC and neglected in NFC. After adding 100% of the moment inertia J, severe disruptions (Test3) just for proposed control based on MRAC because is influenced by parameter changing.

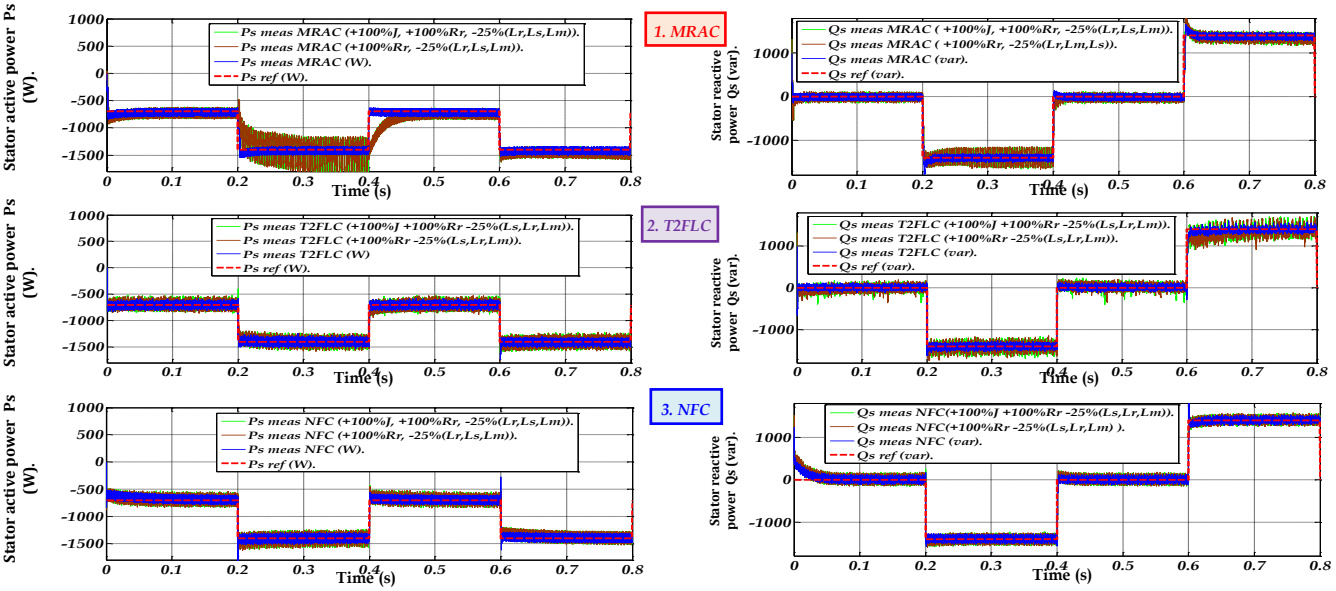

Fig. 13 – Stator active and reactive power based on MRAC, T2FLC and NFC respectively without MPPT strategy.

Fig.13 (to the right) shows the stator reactive power and its reference profiles using SVM for proposed control using MRAC, T2FLC and NFC respectively; the stator active power reference is indicated in table.5. We remark the stator reactive power follows exactly its reference for the three proposed controls (Test1). By using robustness test (Test2) and (Test3), we remark lower undulations in proposed control based on MRAC, T2FLC and neglected in NFC, we note also a remarkable overshoot in proposed control based on NFC and neglected in MRAC, T2FLC. The overshoot existence, the THD of the stator and rotor current and the value of active and reactive power errors (for Test 1), are mentioned in table 2.

We remark that the stator active power follows exactly its reference, for the three proposed controls (Test1). After a robustness test (Test 2), the stator active power follows its reference, but we note that there are ripples in the proposed MRAC and neglected in T2FLC and NFC. After adding +100% of the moment inertia J, a remarkable power error is noted, with severe disruptions; only in the proposed control using MRAC (Test3) because is influenced by parameters changing.

8.2 **CASE II (WITH MPPT STRATEGY):**

Fig.14 (to the left) represents the stator active power injected into the grid using SVM for proposed control using MRAC, T2FLC and NFC respectively, via MPPT strategy.

Fig.14 (to the right) shows the stator reactive power injected into the grid using SVM for proposed control using MRAC, T2FLC and NFC respectively, via MPPT strategy. We remark that the stator reactive power follows exactly its reference (0 var- power factor unity) for the three proposed controls (Test1). By using robustness test (Test2) and (Test 3), we remark remarkable power errors, with severe disruptions and more ripples in proposed MRAC (doesn't maintain 0 var) and power factor (PF) is other than unity, lower in T2FLC and neglected in proposed NFC.

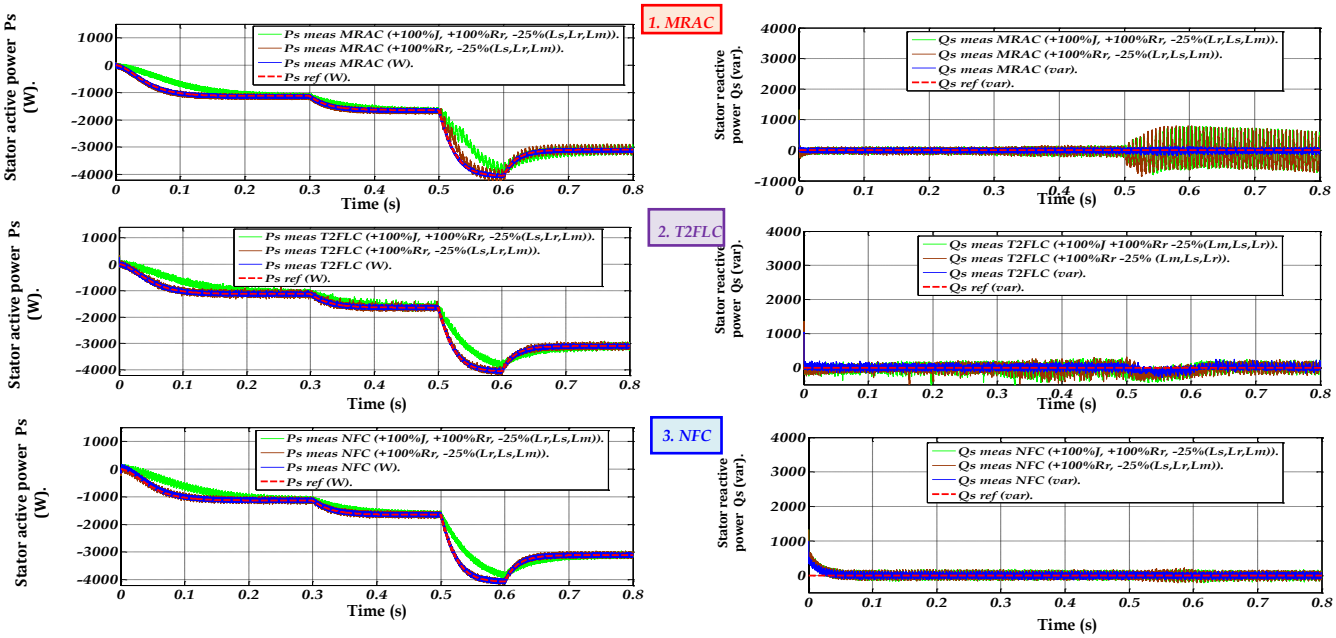

Fig. 14 – Stator active and reactive power based on MRAC, T2FLC and NFC respectively using MPPT strategy

Table 2
Result's Recapitulation

	Proposed Control		
	Based on **MRAC**	Based on **T2FLC**	Based on **NFC**
Overshoot	**A little**	**Neglected**	**A little**
Stator Current's THD	**0.81%**	**1.14 %**	**0.78 %**
Rotor Current's THD	**17.01%**	**13.77%**	**2.80 %**
Power's error	**+/- 120(W_var)**	**+/- 130(W_var)**	**+/- 110(W_var)**

Table 3
Parameters of the DFIG.

Rated Power:	4 kW
Stator Resistance:	Rs = 1.2 Ω
Rotor Resistance:	Rr = 1.8 Ω
Stator Inductance:	Ls = 0.1554 H.
Rotor Inductance:	Lr = 0.1558 H.
Mutual Inductance:	Lm = 0.15 H.
Rated Voltage:	Vs = 220/380 V
Number of Pole pairs:	P= 2
Rated Speed:	N = 1440 rpm
Friction Coefficient:	$fDFIG$ = 0.00 N.m/s
The moment of inertia	J = 0.2 kg.m^2
Slip:	g = 0.015

Table 4
Parameters of the Turbine.

Rated Power:	10 kW
Number of Pole pairs:	P = 3
Blade diameter	R = 3 m
Gain:	G =3.9
The moment of inertia	Jt = 0.00065 kg.m^2
Friction coefficient	ft = 0.017 N.m/s
Air density:	ρ = 1.22 kg/m^3

Table 5
Active and reactive powers references.

Time:	Stator active power Ps:	Stator reactive power Qs:
[0 - 0.2] s	-700 W.	0 var.
[0.2 - 0.4] s	-1400 W.	-1400 var.
[0.4 - 0.6] s	-700 W.	0 var.
[0.6 - 0.8] s	-1400 W.	+1400 var.

9. **CONCLUSION**

In this paper, a new DPC based on hybrid intelligent control for DFIG with SVM has been proposed for wind generation application. DPC via SVM strategy using MPPT strategy has been achieved by adjusting active and reactive powers and rotor currents. The performances of NFC and T2FLC have been investigated and compared to those obtained from the MRAC controller for power control. The results obtained by using the MATLAB/Simulink® using robustness tests (with/without MPPT strategy), have shown that the NFC has high efficiency, lower error, high dynamics for wind generation.

Received on October 16, 2015

REFERENCES

1. Heng Nian, and Yipeng Song, *Direct Power Control of Doubly Fed Induction Generator Under Distorted Grid Voltage*, IEEE Transactions On Power Electronics, Vol. 29, No. 2, February 2014.
2. Heng Nian, Peng Cheng, Z.Q. Zhu, *Coordinated Direct Power Control of DFIG System without Locked Loop under Unbalanced Grid Voltage Conditions*, IEEE Transactions on Power Electronics_2015.
3. Jafar Mohammadi, Sadegh Vaez-Zadeh, Saeed Afsharnia, and Ehsan Daryabeigi, *A Combined Vector and Direct Power Control for DFIG-Based Wind Turbines*, IEEE Transactions on Sustainable Energy, Vol. 5, No. 3, July 2014.
4. Murali M. Baggu, Badrul H. Chowdhury, and Jonathan W. Kimball, *Comparison of Advanced Control Techniques for Grid Side Converter of Doubly-Fed Induction Generator Back-to-Back Converters to Improve Power Quality Performance During Unbalanced Voltage Dips*, IEEE Journal Of Emerging And Selected Topics In Power Electronics, Vol. 03, No. 2, June 2015.
5. Michael K. Bourdoulis, and Antonio T. Alexandridis, *Direct Power Control of DFIG Wind Systems Based on Nonlinear Modeling and Analysis*, IEEE Journal of Emerging and Selected Topics in Power Electronics, Vol. 2, No. 4, December 2014.
6. Bhim Singh, and N. K. Swami Naidu, *Direct Power Control of Single VSC-Based DFIG Without Rotor Position Sensor*, IEEE Transactions On Industry Applications, Vol. 50, No. 6, November/December 2014.
7. Tejavathu Ramesh n, Anup Kumar Panda, S. Shiva Kumar, *Type-2 fuzzy logic control based MRAS speed estimator for speed sensorless direct torque and flux control of an induction motor drive*, ISA Transactions 2015.
8. L. Suganthia, S.Iniyan , Anand A.Samuel , *Applications of fuzzy logic in renewable energy systems – A review*, Renewable and Sustainable Energy Reviews 48, 2015, pp. 585–607.
9. M'hamed Doumi, Abdel Ghani Aissaoui, Ahmed Tahour, Mohamed Abid, *Commande Adaptative D'un Système Éolien*, Rev. Roum. Sci. Techn. – Électrotechn. Et Énerg., 60, 1, pp. 99–110, 2015.
10. Hany M. Jabr, Dongyun Lu, and Narayan C. Kar, *Design and Implementation of Neuro-Fuzzy Vector Control for Wind-Driven Doubly-Fed Induction Generator*, IEEE Transactions On Sustainable Energy, Vol. 2, No. 4, October 2011.
11. Youcef Bekakra and Djilani Ben Attous, *DFIG Sliding Mode Control Driven by Wind Turbine with Using a SVM Inverter for Improve the Quality of Energy Injected into the Electrical Grid*, ECTI transactions on electrical Eng., electronics, and communications vol.11, no.1, pp 36-75, 2013.
12. G. Abad J. Lopez, M.A. Rodrıguez, L. Marroyo, G. Iwanski, *Doubly fed induction machine: modeling and control for wind energy generation*, IEEE press Series on Power Engineering, August 2011.
13. Y. Lei, A. Mullane, G. Lightbody, R. Yacamini, *Modeling of the wind turbine with a doubly-fed induction generator for grid integration studies*, IEEE Trans. Energy Conversion, 21, 1, pp. 257-264, 2006.